ISSN: 2664-9640

Application of sticking-sliding friction model in stainless steel cutting force simulation

Binglin Li, Shidong Geng

School of Mechatronic Engineering, Southwest Petroleum University, Chengdu 610500, China

Abstract

Stainless steel is a difficult to machine material. removing chips from workpiece surface necessitates a lot of cutting force during cutting operation. Cutting parameters and tool geometry parameters are improved by estimating cutting force to increase stainless steel machining precision, chip control, and tool life. A cutting simulation model of the 304 stainless steel cutting force in this paper was established based on numerical modeling method. Sticking-sliding friction model was chosen to improve the accuracy of the developed model. The cutting force results from the literature test were compared to the simulation results. The accuracy of the developed cutting simulation model in this study was estimated for the cutting force of 304 stainless steel, as evidenced by comparison and verification. Finally, cutting force research in this study was carried out under a variety of conditions to improve the cutting efficiency of 304 stainless steel and maintain dimensional accuracy. With an increase in the rake angle and clearance angle of tool and cutting speed, cutting force decreases. However, with an increase in the round radius of cutting edge and the thickness and width of cutting have negative effect. Cutting force is greatly influenced by cutting width, thickness, and rake angle. The work research presented in this paper can provide a theoretical foundation and a technological basis for stainless steel cutting efficiency and cutting mechanism.

Keywords

Stainless steel; Cutting force; Sticking-sliding friction model; finite element simulation.

1. Introduction

As the manufacturing industry grew, the main parts of precision equipment and tools begin to use stainless steel and other difficult materials to improve their performance [1-2]. The surface quality and accuracy of difficult-to-machined materials are required to meet the requirements of safety design standards, sealing, stability, and part life. As a result, cutting difficult-to-machine materials is a critical manufacturing step [3-4]. Analytical modeling, experimental modeling, and numerical modeling are three methods for modeling the cutting process of difficult-to-machine materials. Because the cutting model is excessively complex and the prediction accuracy of the cutting model is low, the analytical modeling method is rarely employed in the real cutting process. Experimental and numerical modeling are commonly used in practical applications. Because of the influence of experimental conditions, it is difficult to change and control the friction state of the tool-chip contact zone and the details of cutting temperature and stress distribution cannot be accurately characterized by experimental modeling method. The cutting process is modeled by numerical modeling method with finite element software. The advantages of analytical and experimental modeling methods are combined to create a simulation model that accurately describes the real cutting process of difficult-to-process materials. This model is useful for studying cutting mechanisms and improving machining accuracy, and it is widely used in practical applications such as cutting

ISSN: 2664-9640

parameter optimization and cutting mechanism analysis [5-6]. Therefore, it is of great practical significance to establish an accurate cutting simulation model for difficult-to-process materials.

Many domestic and international researchers have focused on cutting simulation of difficult-to-process materials since Yoshiaki [7] developed a finite element simulation technique to material cutting research. Various investigations have been carried out in recent years by finite element simulation method, which has become a typical means of the research. Liu et al [8] conducted a three-dimensional machining simulation study for 17-4PH stainless steel, determining the Johnson-Cook constitutive model parameters for 17-4PH stainless steel, and testing the cutting performance of a new curve tool. In the cutting process of AISI 1018, Li et al [9] introduced an improved cutting simulation model and investigated the cutting force and cutting length. Cutting force and the chip contact length of rake face are well predicted by the revised simulation model. To quantitatively analyze the sticking length between chip and tool rake surface, Xu et al [10] conducted research by orthogonal cutting tests and friction tests. They discovered that as cutting speed increased, sliding friction coefficient decreased and sticking length increased. Song et al [11] used finite element approach to establish a cutting model that took into account the built-up layer's size. During dry cutting, the influence of built-up layer size on tool wear of uncoated cemented carbide was investigated. The results reveal that a built-in layer formed at a cutting speed of 40 m/min reduces tool surface wear while having no influence on cutting force amplitude variation and surface roughness. In ultrasonic elliptical vibration cutting of 630 stainless steel, Geng et al [12] proposed a parameter optimization method for work hardening and sensitivity problems. The cutting process of 630 stainless steel was simulated by AdvantEdge software. Cutting force and temperature were studied as a function of cutting speed, feed speed, and cutback. The cutting force and temperature dynamic model were established. Priya et al [13] used finite element modeling method to conduct experiments and two-dimensional and three-dimensional finite element simulations on Martensitic AISI420 steel with coated and uncoated tools for the cutting process of martensitic stainless steel. The research shows that coated cutting tools can reduce the cutting temperature, effective stress, and cutting power consumption of martensitic AISI420 steel.

Despite the fact that a large number of cutting simulation models and tool-chip friction models have been developed by domestic and international scholars to describe the real cutting process of difficult-to-machine materials. However, the cutting mechanism of various difficult-to-machine materials has not been studied. Pure shear friction and Coulomb friction were commonly utilized for the friction between the rake face of tool and chip in cutting simulation studies of difficult-to-process materials. A sticking-sliding friction model and Johnson Cook model were chosen in this research to better characterize the properties of tool-chip friction. Then, the cutting force of orthogonal cutting of 304 stainless steel was simulated. The cutting force calculated by the cutting simulation model was compared with the cutting force acquired by the literature test. Cutting force under different cutting situations was explored through comparison and verification.

2. Establishment of cutting force model

2.1. Material governing equation

The workpiece is made of 304 stainless steel and the Johnson Cook model describes its material attributes as follows:

$$\sigma_q = \left(A + B\varepsilon_q^n\right) \cdot \left(1 + C\ln\left(\frac{\dot{\varepsilon}_q}{\dot{\varepsilon}_o}\right)\right) \cdot \left(1 - \left(\frac{T - T_{it}}{T_{mt} - T_{it}}\right)^m\right) \tag{1}$$

ISSN: 2664-9640

where, σ_q is the shear stress of workpiece, MPa; A is the yield stress of workpiece in initial state, MPa; B is hardening constant, MPa; C is strain rate constant, zero dimension; $\dot{\varepsilon}_q$ is the shear strain rate of workpiece; T is absolute temperature, K; T_{it} is the initial temperature of workpiece, K; T_{mt} is the melting temperature of workpiece, K; $\dot{\varepsilon}_o$ is reference strain rate,s^{-1}; m is softening index, zero dimension; n is hardening index, zero dimension.

The Johnson-Cook parameter values for 304 stainless steel are determined from a reference [14], as indicated in Table 1. Table 2 lists mechanical and thermodynamic features of workpiece and tool materials. Tool is a hard alloy knife without a coating and tool and workpiece will be deformed during cutting process due to mutual extrusion. Because the tool's elastic modulus and density relative to the workpiece are both high, resulting in minimal tool deformation. Therefore, Tool is presumed to be a rigid body.

Table 1 Material parameters of 304 stainless steel Johnson-Cook model

Yield stress /(MPa)	Hardening constant /(MPa)	Strain rate constant /dimensionless	Hardening index /dimensionless	Reference strain rate /(s^{-1})	Softening index /dimensionless	Initial workpiece temperature/(K)	Melting temperature of workpiece/(K)
277	556	0.0096	0.794	0.001	0.944	1673	300

Table 2 Mechanical and thermal parameters of the work-material and of the carbide tool

Name	Elasticity modulus/(GPa)	Poisson's ratio/v	Density/(kg/m^3)	Specific heat capacity /J/(kg·K)	Thermal conductivity /W·m^{-1}·K^{-1}
workpiece	200	0.3	7900	440	16.3
tool	960	0.3	12700	516	33.5

Energy equation analysis can be used to determine the temperature change of workpiece material:

$$\rho_m C_{pm} \dot{T} - k_m \Delta T = \beta d_{ij}^p \sigma_{ij} \tag{2}$$

where, $\dot{T}$ is the material derivative of temperature, K; ρ_m is the density of workpiece, kg/m^3; k_m is the thermal conductivity of workpiece, W·m^{-1}·K^{-1}; ΔT is the Laplace operator of absolute temperature, zero dimension; d_{ij}^p is the component of plastic strain rate tensor, zero dimension; σ_{ij} is the component of Cauchy stress tensor, zero dimension; C_{pm} is the specific heat capacity of workpiece, J/(kg·K).

The governing equation of material properties in the main shear zone can be obtained using momentum conservation, energy conservation, and constitutive relations, where the shear stress at the main shear zone's entrance is σ_0 and the shear stress at the shear zone's exit can be calculated using the motion equation of continuous chip [15]:

$$\sigma_1 = \rho_m \left(v_c \sin \phi_n \cos \lambda_s \right)^2 \gamma_1 + \sigma_0 \tag{3}$$

where, v_c is cutting speed, m/s; λ_s is edge inclination angle, °; ϕ_n is shear angle in the normal plane of tool, °; γ_1 is shear strain at the exit of shear zone; σ_1 is shear stress at the exit of main shear zone, MPa; σ_0 is shear stress at the entrance of main shear zone, MPa.

2.2. Stress distribution on the rake face of took

When tool cuts the workpiece, chip meets tool face and applies normal tension in tool-chip contact area, resulting in sticking friction near tool tip. With the contact area moves away from

ISSN: 2664-9640

tool tip, the normal stress decreases and the friction in the contact area changes to sliding (Coulomb) friction, as shown in Fig. 1. This phenomenon was first proposed by ZOREV[13,16] and expressed as:

$$\begin{cases} \sigma_\mu = \sigma_1, & x \le l_p \\ \sigma_\mu = \mu_s P, & l_p \le x \le l_c \end{cases} \tag{4}$$

where, σ_μ is frictional stress, MPa; x is the distance between knife-chip contact position and tool tip, m; μ_s is sliding friction coefficient, zero dimension. l_p is the length of sticking area, m; l_c is the total length of tool-chip contact area, m; P is normal stress, MPa. The normal stress distribution P(x) was expressed as in the literature [17]:

$$P(x) = P_0\left(1-\frac{x}{l_c}\right)^{\xi} \tag{5}$$

where, ξ is stress distribution index, zero dimension; P_0 is normal stress at the tool tip of rake face, MPa; P_0 can be defined as:

$$P_0 = \frac{\sigma_1 b(\xi+1)\cos\eta_s \cos(\tan\beta\cos\eta_c)}{l_c \sin\phi_n \cos\eta_c \cos(\phi_n + (\tan\beta\cos\eta_c) - \gamma_n)} \tag{6}$$

where, η_s is shear flow angle, °; η_c is chip flow angle, °; γ_n is rake angle, °; b is cutting thickness, m; β is friction angle, °, obtained from β=tan$^{-1}\mu$, μ is apparent friction coefficient, zero dimension. For the contact length between the rake face of tool and chip, it can be separated into two zones: an sticking zone and a sliding zone. The sliding zone length can be determined as follows:

$$l_p = l_c - l_c\left(\frac{\sigma_1}{P_0\mu_s}\right)^{1/\xi} \tag{7}$$

Normal stress is evenly distributed in shear plane, allowing total contact length to be determined using the bending moment balance at the tip:

$$l_c = \frac{b(\xi+2)\sin(\phi_n + (\tan\beta\cos\eta_c) - \gamma_n)}{2\sin\phi_n \cos(\tan\beta\cos\eta_c)\cos\eta_c} \tag{8}$$

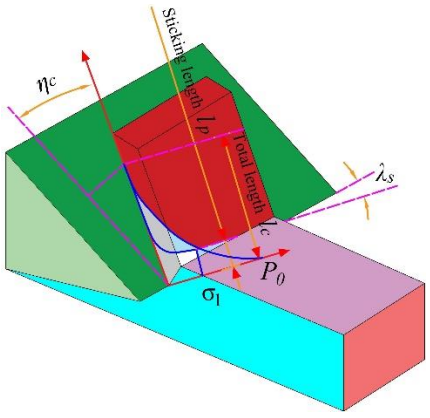

Fig 1 Tool-chip contact diagram

2.3. Calculation of cutting force

According to the approach presented in the literature [18], shear flow angle can be determined as follows:

$$\tan\eta_s = \frac{(\tan\lambda_s \cos(\phi_n - \gamma_n) - \tan\eta_c \sin\phi_n)}{\cos\gamma_n} \tag{9}$$

ISSN: 2664-9640

For the mentioned apparent friction coefficient μ and sliding friction coefficient μ_s, there is the following relationship [19]:

$$\mu=\frac{\sigma_1}{P_0}\left[1+\xi\left(1-\left(\frac{\sigma_1}{P_0\mu_s}\right)^{1/\xi}\right)\right] \tag{10}$$

This is a right-angle cutting model where edge inclination angle is zero. The cutting force F_t and feed force F_f parallel to cutting speed can be calculated using the balance of forces operating on chips, as shown in Fig. 2.

$$\begin{cases} F_t=\dfrac{\sigma_1 bw\cos\left(\left(\tan\beta\cos\eta_c\right)-\gamma_n\right)}{\sin\phi_n\cos\left(\phi_n+\left(\tan\beta\cos\eta_c\right)-\gamma_n\right)} \\ F_f=\dfrac{\sigma_1 bw\sin\left(\left(\tan\beta\cos\eta_c\right)-\gamma_n\right)}{\sin\phi_n\cos\left(\phi_n+\left(\tan\beta\cos\eta_c\right)-\gamma_n\right)} \end{cases} \tag{11}$$

where, w is cutting width, m.

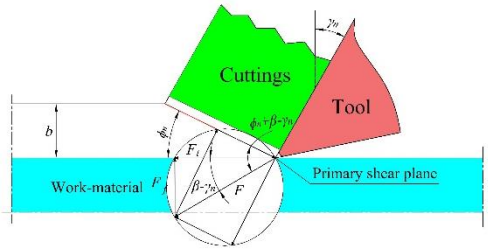

Fig 2 Cutting force analysis

3. Simulation modeling and validation analysis

3.1. Simulation modeling

Because any local chip flow direction is perpendicular to cutting edge in the orthogonal cutting process of 304 stainless steel. Cutting width is significantly bigger than the feed and three-dimensional orthogonal cutting can be simplified into two-dimensional orthogonal cutting [20]. Fig. 3 depicts the 2D orthogonal cutting geometric model of 304 stainless steel. Workpiece is 15 mm long and 9 mm wide. The rake angle of tool is 15 °. The clearance angle of tool is 10 °. The edge inclination angle of tool is 0 ° The round radius of cutting edge is 0.01mm.

In this paper, a quadrilateral structural mesh was used to describe a two-dimensional orthogonal cutting geometric model in which workpiece is separated into three layers: cutting layer, transition layer, and fixed layer. The cutting part's mesh size is 0.1mm and the tool's rake face, flank face, and tip are refined. The rest of the mesh is sparse. Temperature-displacement coupling element is a tool and workpiece element attribute.

In the first half of this work, the friction of the tool-chip contact face in the cutting simulation model was thoroughly examined. In the sticking zone and the sliding zone, sliding friction coefficient is 0.6 and final surface residual stress cloud is illustrated in Fig. 3.

ISSN: 2664-9640

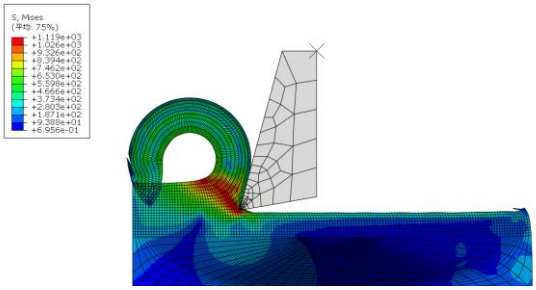

Fig 3 Equivalent stress distribution

3.2. Check analysis

The orthogonal cutting experiment of 304 stainless steel on a horizontal lathe was carried out in the literature[14] to test the accuracy of the cutting simulation model in this research. The tool in the experiment have a 3 mm cutting width and a 0° rake angle. Experiments and simulation calculations on cutting forces at cutting speeds of 66 m/min, 95 m/min, and 138 m/min were carried out and the results were compared using average value. The error control of the cutting simulation model in this paper, as shown in Table 3, is within a reasonable range. The cutting simulation model is more consistent with the experimental results when the cutting speed and thickness are low.

Table 3 Comparison of results

Number	Cutting speed /(m/min)	Cutting speed /(mm)	Cutting force/(N)		Error /(%)
			Experiment	Prediction	
1	66	0.075	1397	1368.45	2.04
2	95	0.1	1474	1355.15	8.06
3	138	0.2	1198	1017.71	15.05

This paper chose sticking-sliding friction model, which can better describe the tool-chip friction characteristics, to simulate and optimize the cutting process of 304 stainless steel and performs simulation prediction for cutting force to improve the accuracy of the cutting simulation model. In the optimized cutting simulation model, the prediction results of pure shear friction or Coulomb friction are presented in Fig. 4. Cutting force predicted by stick-slip friction model is closer to the experimental data, as seen in Fig. 4. Stick-slip friction model is accurate in describing the features of tool-chip friction than pure shear friction and Coulomb friction.

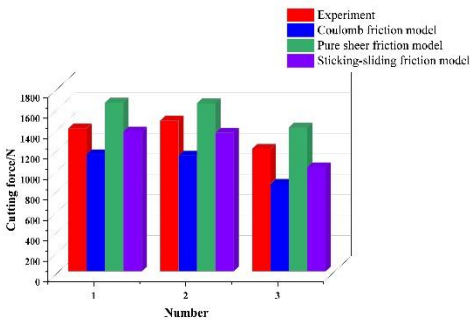

Fig 4 Comparison of cutting force results for different friction models

ISSN: 2664-9640

4. Sensitivity analysis

Predicting cutting force is critical in cutting process for optimizing cutting parameters, tool parameters, ensuring tool life, enhancing machining precision, and cutting regulation. Therefore, it's critical to investigate the impact of various parameters on cutting force. The following parameters were used in sensitivity analysis. The rake angle of tool is 15 °. The clearance angle of tool is 10 °. The cutting speed of tool is 66 m/min. Cutting thickness is 1 mm/r. Cutting width is 3 mm. Sliding friction coefficient is 0.6.

4.1. Influence of cutting width on cutting force

As shown in Fig. 5, with an increase in cutting width, cutting force increases, mainly because an increase in cutting width leads to an increase in the contact area between the rake face of tool and chip. Therefore, with an increase in friction stress, cutting force increases. The plastic deformation region of material increases.

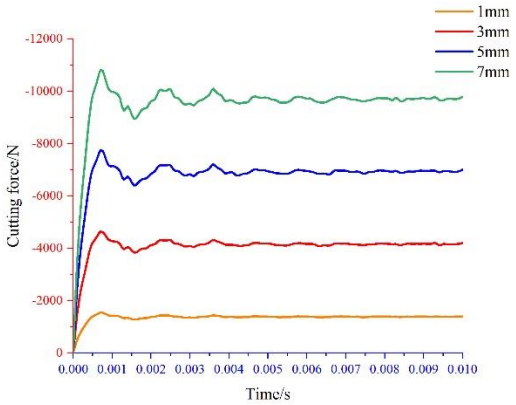

Fig 5 Cutting force varies with the cutting width

4.2. Influence of cutting thickness on cutting force

As shown in Fig. 6, with an increase in cutting thickness, cutting force increases, mainly because an increase in cutting thickness leads to an increase in the resistance of the rake face of tool to the material. Therefore, with an increase in normal stress on the rake face of tool, the friction stress of tool-chip contact area increases, resulting in an increase in cutting force.

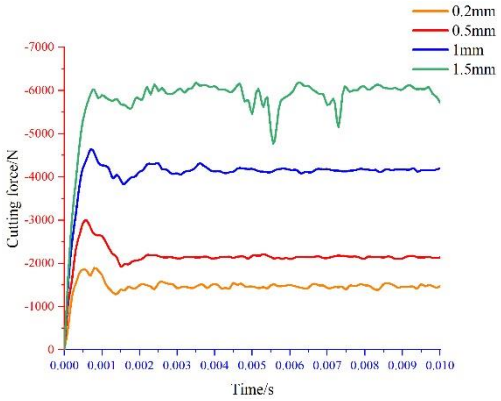

Fig. 6. Cutting force varies with cutting thickness

4.3. Influence of cutting speed on cutting force

As shown in Fig. 7, with an increase in cutting speed, a decrease in cutting force, mainly because an increase in cutting speed leads to plastic deformation being slower than elastic deformation, resulting in insufficient cutting deformation and a decrease in deformation coefficient. Meanwhile, an increase in cutting temperature leads to the thermal softening of workpiece and tool and a decrease in friction coefficient. Therefore, cutting force decreases.

ISSN: 2664-9640

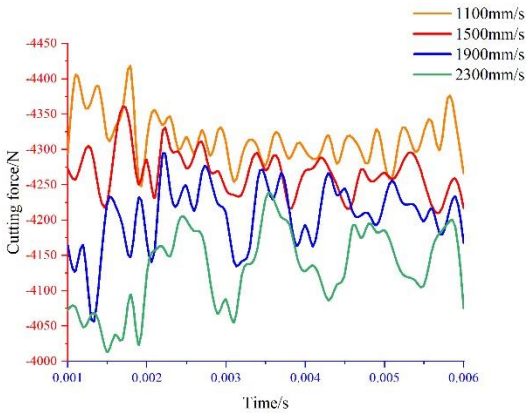

Fig. 7. Cutting force varies with the cutting speed

4.4. Influence of rake angle on cutting force

As shown in Fig. 8, with an increase in the rake angle of tool, cutting force decreases, mainly because an increase in the rake angle of tool leads to an increase in shear angle and a decrease in friction angle. Therefore, the extrusion of tool decreases. The plastic deformation and friction stress of workpiece cutting layer decrease and cutting force decreases. However, the increase of the rake angle of tool will thin cutting edge and decrease tool strength.

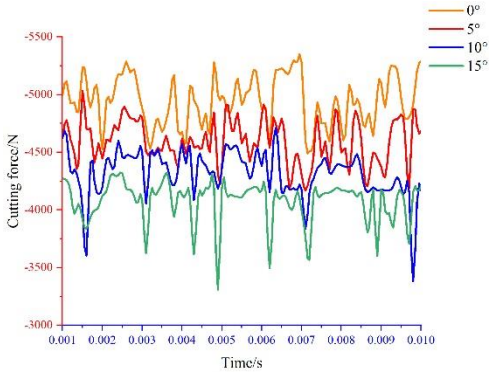

Fig. 8. Cutting force varies with rake angle

4.5. Influence of clearance angle on cutting force

As shown in Fig. 9, with an increase in the clearance angle of tool, cutting force decreases, mainly because an increase in the clearance angle of tool leads to a better cutting edge and the friction between the flank face of tool and machined surface decreases. Cutting force decreases, but the increase in the clearance angle of tool will also decrease the tool strength. The clearance angle of tool has little effect on cutting force.

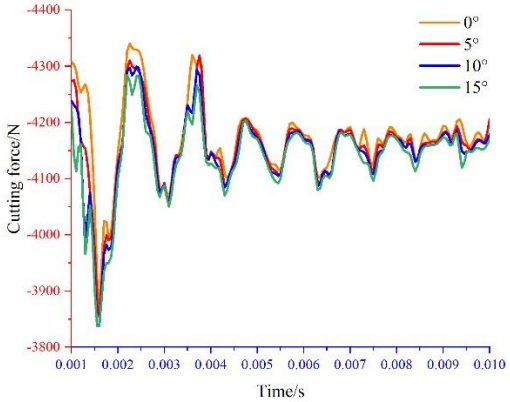

Fig. 9. Cutting force varies with clearance angle

ISSN: 2664-9640

4.6. Influence of round radius of cutting edge on cutting force

As shown in Fig. 10, with an increase in the round radius of cutting edge, cutting force increases, mainly because an increase in the round radius of cutting edge leads to an increase in the functional proportion of the round radius of cutting edge and the effect of ploughing on entire cutting surface. With an increase in cutting force, the actual rake angle of tool on cutting edge decreases, but the contribution of ploughing to cutting force is usually minor. Therefore, the round radius of cutting edge has little effect on cutting force.

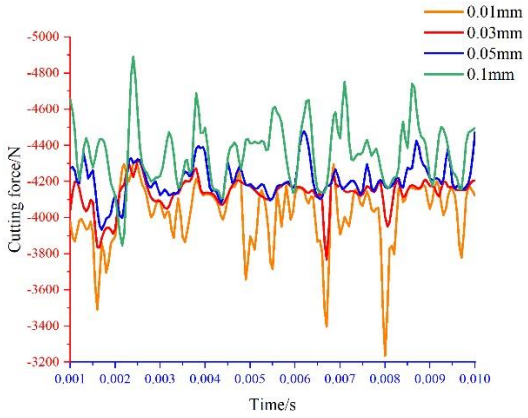

Fig.10. Cutting force varies with round radius of cutting edge

5. Conclusion

Stainless steel is an example of a difficult-to-process material. A cutting simulation model for 304 stainless steel was constructed in this article and a sticking-sliding friction model was used to optimize the simulation model, which can better explain the tool-chip friction characteristics. Cutting force determined by the cutting simulation model was compared to cutting force determined by the literature test. It has been confirmed through comparison and verification that the cutting simulation model developed in this work was accurate in simulating the cutting force of 304 stainless steel. Finally, a sensitivity analysis of parameters was performed. The results show that cutting width, thickness, and rake angle of tool have influence on cutting force. They should be used primarily for adjusting the change in cutting force during actual cutting operations, but they should also consider the influence of cutting speed, round radius of cutting edge, and clearance angle on cutting force, after designing reasonable tool geometric parameters and cutting parameter optimization designs, to improve the machining accuracy and cutting efficiency of 304 stainless steel. The work research presented in this paper can provide a theoretical foundation and a technological basis for stainless steel cutting efficiency and cutting mechanism.

References

[1] M.Mohammad, D.B. Camilla, A.Z. Maryam, et al. Cutting edge wear in high-speed stainless steel end milling. The International Journal of Advanced Manufacturing Technology, 114(9-10) (2021): 2991-2928. https://doi.org/10.1007/s00170-021-07006-5.

[2] N. Rusdi, M.Y. Noordin, S. Izman, et al. Determination of energy consumption during turning of hardened stainless steel using resultant cutting force. Metals, 11(4) (2021): 565. https://doi.org/10.3390/met11040565.

[3] Z.M. Magdlena, P. Pawel, J. Jerzy. Tribological aspects of cutting tool wear during the turning of stainless steels. Materials, 13(1) (2020): 123. https://doi.org/10.3390/ma13010123.

[4] M. Achim, B. Madlen, P. Peer. Factorial analysis of fiber laser fusion cutting of AISI 304 stainless steel: evaluation of effects on process performance, Kerf Geometry and Cut Edge Roughness. Materials, 14(10) (2021): 2669. https://doi.org/10.3390/ma14102669.

[5] Y.S. Xu, Z.H. Wan, P. Zou, et al. Experimental study on cutting force in ultrasonic vibration-assisted turning of 304 austenitic stainless steel. Proceedings of the Institution of Mechanical Engineers, 235(3) (2021): 494-513. https://doi.org/10.1177/0954405420957127.

[6] A. Paulo, F. Pedro, S. Fernando. Comparative analysis of different cutting milling strategies applied in duplex stainless steel. Procedia Manufacturing, 47(2020): 517-524. https://doi.org/ 10.1016/j.promfg.2020.04.132.

[7] K. Yoshiaki. Analysis of the mechanism of orthogonal machining by the finite element method. Journal of the Japan Society for Precision Engineering, 37(438) (1971): 503-508.https://doi.org/ 10.2493/jjspe1933.37.503.

[8] G.L. Liu, C.Z. Huang, R. Su, et al. 3D FEM simulation of the turning process of stainless steel 17-4PH with differently texturized cutting tools. Proceedings of the Institution of Mechanical Engineers, Part B: Journal of Engineering Manufacture, 234(8) (2020): 1113-1123. https://doi.org/10.1016/ j.ijmecsci.2019.03.016.

[9] X. Li, Z.Y. Shi, N.M. Duan. Cutting performance investigation based on the variable friction model by considering sliding velocity and limiting stress. Proceedings of the Institution of Mechanical Engineers, Part B: Journal of Engineering Manufacture, 2020, 234(8): 1113-1123.

[10] M.X. Li, D.C. Xu, Z.Y. Cui, et al. Research on the sticking-sliding contact ratio in high-speed cutting of cupronickel B10. Journal of Mechanical Science & Technology, 34(3) (2020): 1275-1282. https://doi.org/10.1007/s12206-020-0226-0.

[11] X.Q.Song, T. Yukio, H.E. Weiming, et al. Effects of the size of built-up layer on the wear of cemented carbide tools in cutting of SUS304 stainless steel. Journal of Advanced Mechanical Design, Systems, and Manufacturing, 15(4) (2021): JAMDSM0050. https://doi.org/ 10.1299/ jamdsm. 2021 jamdsm0050.

[12] G.S. Geng, Y. Wang, L. Zhang, et al. Optimization of cutting parameters in double-excitation ultrasonic elliptical vibration cutting of 630 stainless steel. The International Journal of Advanced Manufacturing Technology, 114(7-8) (2021): 2169-2183. https://doi.org/10.1007/s00170-021-06939-1.

[13] R. priya, S. Somashekhar. Finite element simulation and experimental validation of machining martensitic stainless steel using multi-layered coated carbide tools for industry-relevant outcomes. Simulation Modelling Practice and Theory, 144(2022): 102411. https://doi.org/10.1016/j. simpat.2021.102411.

[14] B.L. Li. Research on analytical prediction of cutting forces in stainless steel machining. Hebei: Huazhong University of Science &Technology, 2012.

[15] A. Malinari, R. Cheriguene, H. Miguelez. Contact variables and thermal effects at the tool–chip interface in orthogonal cutting. International Journal of Solids and Structures, 49(26) (2012): 3774-3796. https://doi.org/10.1016/j.ijsolstr.2012.08.013.

[16] N.N. Zorev. Inter-relationship between shear processes occurring along tool face and shear plane in metal cutting. International Research in Production Engineering. New York: ASME, 1963: 42-49.

[17] B.C. behera, S. Ghosh, P.V. Rao. Modeling of cutting force in MQL machining environment considering chip tool contact friction. Tribology International, 117(1) (2018): 283-295. https://doi.org/10.1016/j.triboint.2017.09.015.

[18] M.E. Merchant. Basic Mechanics of the metal-cutting process. Transactions of the ASME Journal of Applied Mechanics, 11(3) (1994): 75-168. https://doi.org/10.1115/1.4009380.

[19] E. Ozlu, E. Budak, A. Molinari. Thermomechanical modeling of orthogonal cutting including the effect of stick-slide regions on the rake face. University of Calabria, 2007, 8. https:// www.researchgate.net/publication/277792992.

[20] C.W. Shan, X. Zhang, B. Shen, et al. An improved analytical model of cutting temperature in orthogonal cutting of Ti6Al4V. Chinese Journal of Aeronautics, 32(03) (2019): 759-769. https://doi.org/10.1016/j.cja.2018.12.001.